

Evolution of Electronic Structure in Atomically Thin Sheets of WS₂ and WSe₂

Weijie Zhao^{a,c,#}, Zohreh Ghorannevis^{a,c,#}, Leiqliang Chu^{a,c}, Minglin Toh^d, Christian Kloc^d, Ping-Heng Tan^e, Goki Eda^{a,b,c,}*

^a Department of Physics, National University of Singapore, 2 Science Drive 3, Singapore 117542

^b Department of Chemistry, National University of Singapore, 3 Science Drive 3, Singapore 117543

^c Graphene Research Centre, National University of Singapore, 6 Science Drive 2, Singapore 117546

^d School of Materials Science and Engineering, Nanyang Technological University, N4.1 Nanyang Avenue, Singapore 639798

^e State Key Laboratory of Superlattices and Microstructures, Institute of Semiconductors, Chinese Academy of Sciences, Beijing 100083, China

* E-mail: g.eda@nus.edu.sg

These authors contributed equally to this work.

Abstract

Geometrical confinement effect in exfoliated sheets of layered materials leads to significant evolution of energy dispersion with decreasing layer thickness. Molybdenum disulphide (MoS₂) was recently found to exhibit indirect to direct gap transition when the thickness is reduced to a single monolayer. This leads to remarkable enhancement in the photoluminescence efficiency, which opens up new opportunities for the optoelectronic applications of the material. Here we report differential reflectance and photoluminescence (PL) spectra of mono- to few-layer WS₂ and WSe₂ that indicate that the band structure of these materials undergoes similar indirect to direct transition when thinned to a single monolayer. Strong enhancement in PL quantum yield is observed for monoayer WS₂ and

WSe₂ due to exciton recombination at the direct band edge. In contrast to natural MoS₂ crystals extensively used in recent studies, few-layer WS₂ and WSe₂ show comparatively strong indirect gap emission along with distinct direct gap hot electron emission, suggesting high quality of synthetic crystals prepared by chemical vapor transport method. Fine absorption and emission features and their thickness dependence suggest strong effect of Se p-orbitals on the d electron band structure as well as interlayer coupling in WSe₂.

Keywords: WS₂, WSe₂, 2D crystals, photoluminescence

Atomically thin sheets of MoS₂ consisting of a single to a few monolayers were recently found to exhibit a set of unusual properties associated with its two dimensional (2D) structure and high crystal quality, triggering significant research interest.¹⁻¹⁸ Similar to graphite, MoS₂ crystallizes in a van der Waals layered structure where each layer consists of a slab of S-Mo-S sandwich. Individual monolayers can be mechanically peeled off from a bulk crystal and isolated as graphene-like 2D crystal.¹⁹ While MoS₂ is traditionally known as solid-state lubricant and catalyst, its monolayer crystal hold promise in novel electronic and optoelectronic applications as well as provide access to fundamental physical phenomena. Electronically, a bulk MoS₂ is an indirect gap semiconductor with the bandgap in the near-infrared frequency range (~ 1.2 eV).²⁰ In contrast, monolayer MoS₂ is a direct gap semiconductor with the band gap in the visible frequency range (~ 1.9 eV).⁴⁻⁵ Confinement of carriers in the out-of-plane direction induces gradual increase in the band gap with decreasing thickness.²¹ The indirect to direct crossover occurs at the monolayer limit resulting in strong contrast in photoluminescence (PL) efficiency between single and multilayer sheets.⁴⁻⁵ Remarkable electrical properties of mono- and few-layer MoS₂ are increasingly revealed in its field effect transistor characteristics such as exceptionally large on/off ratio, small subthreshold swing, ultra-low off-state energy dissipation, high field effect mobility, and large current carrying capacity.¹⁻³ Explicit inversion symmetry breaking in monolayers allows valley selective pumping of charges using circularly polarized light.⁶⁻⁸ High electronic quality of the material coupled with thickness dependent optical properties, mechanical flexibility,⁹ and access to valley degree of freedom highlights some of the distinct characteristics of atomically thin MoS₂.¹⁰⁻¹⁸

Tungsten-based dichalcogenides such as WS₂ and WSe₂ belong to the same family of layered transition metal dichalcogenides (LTMD) as MoS₂.²² Mechanically exfoliated atomically thin sheets of WS₂ and WSe₂ were recently shown to exhibit high in-plane carrier mobility and electrostatic modulation of conductance similar to MoS₂.²³⁻²⁴ Both compounds exhibit trigonal prismatic structure and are indirect gap semiconductors in the bulk form with a bandgap of ~ 1 eV as MoS₂. The lattice constants are nearly identical for MoS₂ (3.16 Å)

and WS_2 (3.15 Å) while WSe_2 exhibits a slightly larger value (3.28 Å).²² Interlayer distance is correspondingly larger for WSe_2 due to the large size of Se atom. General features of the WS_2 and WSe_2 band structures are similar to those of MoS_2 where a direct and indirect gap coexist irrespective of thickness.²⁵⁻²⁷ Direct gap exists at the K points of the Brillouin zone between spin-orbit split valence band and doubly degenerate conduction band. On the other hand, indirect gap forms between a local conduction band minimum at a midpoint between Γ and K and valence band maximum at the Γ point. The primary difference between MoX_2 (where X represents chalcogen atoms) and WX_2 is the size of the spin-orbit splitting due to the different size of the transition metal atom.

While MoS_2 2D crystals have been extensively studied recently, understanding of confinement effects on WS_2 and WSe_2 in the mono- to few-layer thickness regimes is limited. Here we report the evolution of optical absorption and PL spectra of mechanically exfoliated sheets of synthetic 2H- WS_2 and 2H- WSe_2 with thicknesses ranging between 1 and 5 monolayers. The excitonic absorption and emission bands were found to gradually blueshift with decreasing number of layers due to geometrical confinement of excitons. Strong enhancement in PL efficiency is observed in monolayers indicating that they are direct gap semiconductors in agreement with the recent experimental findings²⁸⁻²⁹ and calculations.²⁵⁻²⁶ We show that interlayer coupling effects can be investigated by studying fine absorption and emission features and their dependence on sample thickness. We further demonstrate that the PL emission efficiency of monolayers is higher for synthetic WS_2 and WSe_2 crystals compared to natural MoS_2 crystals.

Results/Discussion

Mechanically exfoliated flakes of WS_2 and WSe_2 were deposited on quartz or SiO_2/Si substrates and their thickness was verified by atomic force microscopy (AFM) and optical contrast (See Supporting Information for AFM images).³⁰ These samples were chemically stable over 3 months in ambient conditions and showed no obvious sign of degradation according to our Raman analysis.³¹ For atomically thin layers supported by a transparent

substrate, differential reflectance provides an effective measure of absorbance. Fractional change in reflectance δR for a thin layer sample relative to the reflectance of a dielectric substrate with refractive index of n_{subs} is related to the absorbance (A) of the material by³²

$$\delta_R(\lambda) = \frac{4}{n_{\text{subs}}^2 - 1} A(\lambda). \quad (1)$$

We assume n_{subs} to be wavelength independent for the spectral range investigated in this study. Figures 1a and 1b show the differential reflectance spectra of 1-5 layer WS_2 and WSe_2 , respectively. Absorption features for bulk crystals have been previously studied by Beal *et al.*³³ and Bromley *et al.*³⁴ General features of the peaks are in good agreement with previously reported results. All peaks exhibit gradual but distinct blueshift with decreasing sample thickness similar to early findings.³⁵ Excitonic absorption peaks A and B which arise from direct gap transitions at the K point are found, respectively, around 625 nm and 550 nm for WS_2 and around 760 nm and 600 nm for WSe_2 in agreement with the previous studies on bulk layers.³³⁻³⁴ The energy difference between the A and B peaks, which is an indication of the strength of spin-orbit interaction, is approximately 400 meV for both WS_2 and WSe_2 in reasonable agreement with the calculations.³⁶ It should be noted that this value is significantly larger than the ~ 160 meV splitting observed for MoS_2 .⁴⁻⁵

For WS_2 , an additional peak, previously labeled as C, is observed around 450 nm. This peak arises from optical transitions between the density of states peaks in the valence and conduction bands.³⁷ The WSe_2 spectra show more additional features due to greater overlap of anion p orbitals with tungsten d orbitals as well as those of adjacent layers.³³⁻³⁴ The absorption peaks A' and B' are believed to be excitonic in nature and arise from splitting of the ground and excited states of A and B transitions, respectively, due to inter- and intra-layer perturbation to the d electron band by the Se p orbitals.³³⁻³⁴ The energy separation between A' and B' peaks are found to be ~ 400 meV consistent with this picture. It may be noted that the presence of A' and B' peaks in monolayer WSe_2 suggests that A-A' and B-B' splitting are mainly due to intralayer effects.

In contrast to absorption, PL spectra show remarkable dependence on sample thickness for both materials as shown in Figure 2a and b. The most notable change was a sudden increase in emission intensity when the sample was thinned to a monolayer (Figure 2c and d). Both monolayer WS₂ and WSe₂ samples exhibited distinct emission at the energy corresponding to A excitonic absorption whereas the emission intensity was dramatically reduced for multilayer samples. While an accurate measurement of the PL quantum yield (QY) is challenging, relative changes in QY between different samples can be evaluated based on the PL and absorption spectra. Since the integrated PL intensity I is proportional to the product of $\alpha(\lambda_{\text{exc}})$ and QY, where $\alpha(\lambda_{\text{exc}})$ is the absorption coefficient at the excitation wavelength λ_{exc} , we can evaluate the relative magnitude of QY by comparing $I/\alpha(\lambda_{\text{exc}})$. Figure 2c and d show relative decrease in PL QY with respect to monolayer samples. For WS₂, PL QY drops by more than 100 folds when the thickness is increased from monolayer to bilayer and gradually diminishes with further increase in thickness. A similar jump in PL QY was observed for WSe₂ despite with less pronounced contrast between monolayer and bilayer samples.

For A excitonic emission from monolayer WS₂ and WSe₂, Stokes shift was typically around 20 meV and 3 meV and the corresponding full width at half maximum (FWHM) for these peaks was 75 meV and 26 meV, respectively (See Supporting Information for details). It is known that for quantum well structures Stokes shift as well as emission linewidth are an indication of interfacial quality.³⁸ A recent study showed that the size of Stokes shift in monolayer MoS₂ increases with doping concentration.³⁹ The narrow emission line, whose FWHM is comparable to thermal energy at room temperature, along with the small Stokes shift indicates high quality of our WSe₂ samples.

In addition to the A exciton peak, another peak at a longer wavelength was observed for multilayer samples of both materials. This is attributed to indirect band gap emission involving conduction band minimum at a midpoint between K and Γ points and valence band maximum at the Γ point. Calculations show that for WSe₂ bilayers, the indirect gap emission involves valence band maximum at the K point which is nearly degenerate with the band

maximum at the Γ point.^{26, 40} It should be noted that the indirect gap emission peak is virtually absent in the monolayer emission spectra, indicating that both WS_2 and WSe_2 become a direct gap semiconductor when they are thinned to a single monolayer. This observation along with the distinctly strong emission from monolayers is in good agreement with the calculated²⁵⁻²⁷ results as well as very recent experimental findings.²⁸

We observed that the decay in emission intensity with increasing thickness is more moderate for WSe_2 compared to WS_2 . This is attributed to the small difference between the direct and indirect emission energies. For bulk WSe_2 , the energy difference between the Γ and K points of the valence band was previously measured by photoemission spectroscopy to be < 80 meV.⁴¹⁻⁴² Theoretical calculations also yield similar results^{26, 40}. For bilayer WSe_2 , the difference between the direct and indirect gaps is a measure of the energy separation between the conduction minimum at the K point and at a midpoint between Γ and K points. Based on our PL results we find this energy separation in bilayer WSe_2 to be about 70 meV. In comparison, the difference between the indirect and direct band gaps in bilayer WS_2 is much greater (~ 300 meV). Because the population of hot electrons that transiently occupy the direct band edge at the K point is higher in bilayer WSe_2 due to the smaller energy difference between its direct and indirect gaps, its A exciton hot electron emission is pronounced. A similar scenario was recently reported for few-layer MoSe_2 .⁴³

For multilayer samples, the indirect gap emission intensity is comparable to or higher than that of hot electron emission from A excitons. We compared the indirect gap emission intensity of commercially available natural MoS_2 and our tungsten dichalcogenides grown by CVT and found that the emission intensity was distinctly higher for synthetic WS_2 and WSe_2 . Radiative recombination across an indirect gap is a slow process requiring phonons with an appropriate momentum. In the presence of defects acting as nonradiative traps, nonradiative decay will dominate and suppress the PL QY. Observation of comparatively strong indirect gap emission therefore provides further evidence that our CVT-grown samples are of high quality.

Figure 3 shows absorption and PL peak energies as a function of the number of layers for WS₂ and WSe₂. The A and B exciton peak positions are only weakly dependent on the sample thickness while the indirect band gap energy quickly increases with decreasing thickness similar to the case of MoS₂. The robust direct gap at the K point is a consequence of absence of dispersion in the out-of-plane direction (or large effective mass in the out-of-plane direction). On the other hand, out-of-plane dispersion at the Γ point and along Γ -K line is greater and results in thickness dependent indirect gap. Therefore, large shift in absorption and emission peaks with flake thickness is an indication of strong out-of-plane dispersion or interlayer coupling of the electronic states. The energy of A, B, and C peaks in WS₂ are weakly dependent on the flake thickness indicating that the d electrons localized around the metal atoms are responsible for these optical transitions. For WSe₂, the shift in peaks A' and B' are more pronounced compared to that of peaks A and B suggesting that the electronic states associated with these optical transitions are more delocalized across the layers.

Photoluminescence from monolayer flakes were sufficiently strong to be imaged under fluorescence microscope. Figure 4 shows bright field optical microscope images and corresponding fluorescence images of exfoliated WS₂ and WSe₂ on quartz substrates. The fluorescence images clearly show that monolayer regions are luminescent in red consistent with the emission spectrum. Emission intensity from the adjacent bilayer regions is not sufficiently strong to be detected by the camera. The emission intensity is uniform across the monolayer region, verifying that emission is not due to anomalies arising from flake edges. Similar fluorescence images were obtained for samples deposited on SiO₂/Si substrates (See Supporting Information). These results demonstrate that fluorescence imaging offers a powerful tool to quickly identifying monolayers.

Ideal direct band gap semiconductors are expected to exhibit high PL QY. However, PL QY of MoS₂ monolayer was previously found to be extremely low (4×10^{-3}).⁵ The origin of the low QY is yet to be understood. Unintentional doping in the natural crystals with an estimated concentration of $\sim 10^{12} \text{ cm}^{-2}$,^{6, 18} may play a role in suppressing radiative

recombination in addition to crystal defects. Figure 5 shows a relative comparison of the emission intensity from the three materials. The emission efficiency of our monolayer WS_2 and WSe_2 is 20 to 40 times higher than that of monolayer MoS_2 obtained from a natural crystal. The emission from bilayer WSe_2 is also more efficient in comparison to monolayer MoS_2 . The differences in PL QY may arise due to various intrinsic and extrinsic factors. Doping is expected to play a major role in suppressing PL in monolayers.⁴⁴⁻⁴⁵ Since the materials studied here are unintentionally doped at different concentrations, we suspect that the observed differences mainly arise from doping. Further studies are required to elucidate the origin of the variation in PL QY reported here.

Conclusions

In summary, we studied the evolution of electronic structure in atomically thin WS_2 and WSe_2 sheets using differential reflectance and PL spectroscopy. Our results demonstrate that indirect to direct crossover occurs in these materials when they are thinned to a single monolayer similar to the case of MoS_2 . Due to the excitonic recombination at direct band gap, distinct and intense PL centered at 630 nm and 750 nm is observed from monolayer WS_2 and WSe_2 , respectively, which is 100 to 1000 times stronger than that in indirect-gap bulk materials. High quality of our CVT-grown samples are suggested by the distinct indirect gap emission, small Stokes shift and narrow emission linewidth. Strong interlayer coupling in WSe_2 is evidenced by the presence of A' and B' absorption and emission peaks and their strong thickness-dependent shift.

Our findings demonstrate the unique variations in the optical properties of 2D semiconducting crystals belonging to the family of Group 6 TMDs. Structural similarities of these materials will allow fabrication of coherent artificial crystals consisting of electronically dissimilar layers.⁴⁶⁻⁴⁸ Monolayer WS_2 and WSe_2 with direct band gap in the visible and NIR frequency ranges, respectively, are novel building blocks for realizing unique

heterostructures with tailored optoelectronic, electrocatalytic, and photocatalytic functionalities.⁴⁹

Method

Synthetic crystals of 2H-WS₂ and 2H-WSe₂ were grown by chemical vapor transport (CVT) method using iodine as the transport agent. Commercial natural 2H-MoS₂ (SPI Supplies) was studied for comparison. The crystals were mechanically exfoliated and deposited on quartz and SiO₂/Si substrates for subsequent characterizations. Regions of the sample containing mono- and few-layer sheets were first identified under optical microscope and the number of layers was verified by atomic force microscope (AFM) and optical contrast. Differential reflectance measurements were performed in a backscattering geometry using a Jobin-Yvon HR800 micro-Raman system equipped with a liquid nitrogen cooled charge-coupled detector. A tungsten-halogen lamp was used as a light source. The differential reflectance is defined as $1-R_S/R_Q$, where R_S and R_Q are the reflected light intensities from the quartz substrate with and without WS₂/WSe₂ flake samples, respectively. The light illuminating the sample was focused down to 1 μm spot using a small confocal hole. The spectra acquisition time was 15s. The intensity of the light incident on the sample was kept low (< 1 mW) in order to avoid sample damage. Photoluminescence spectra were obtained in a back scattering geometry with a 473 nm excitation laser at intensities less than 150 μW. The fluorescence images were obtained with an Olympus fluorescence microscope equipped with a Mercury lamp as the excitation light source.

Acknowledgements

G Eda acknowledges Singapore National Research Foundation for funding the research under NRF Research Fellowship (NRF-NRFF2011-02). PH Tan thanks the supports from NSFC under grants 10934007 and 11225421.

Supporting Information Available

Atomic force microscope (AFM) results, fluorescence microscope images, and additional photoluminescence spectra showing Stokes shift are presented. This material is available free of charge via the Internet at <http://pubs.acs.org>.

References

1. Radisavljevic, B.; Radenovic, A.; Brivio, J.; Giacometti, V.; Kis, A., Single-Layer Mos₂ Transistors. *Nat. Nanotechnol.* **2011**, *6*, 147-150.
2. Lembke, D.; Kis, A., Breakdown of High-Performance Monolayer Mos₂ Transistors. *ACS Nano* **2012**, *6*, 10070–10075.
3. Liu, H.; Neal, A. T.; Ye, P. D., Channel Length Scaling of Mos₂ Mosfets. *ACS Nano* **2012**, *6*, 8563-8569.
4. Splendiani, A.; Sun, L.; Zhang, Y.; Li, T.; Kim, J.; Chim, C.-Y.; Galli, G.; Wang, F., Emerging Photoluminescence in Monolayer Mos₂. *Nano Lett.* **2010**, *10*, 1271-1275.
5. Mak, K. F.; Lee, C.; Hone, J.; Shan, J.; Heinz, T. F., Atomically Thin Mos₂: A New Direct-Gap Semiconductor. *Phys. Rev. Lett.* **2010**, *105*, 136805.
6. Mak, K. F.; He, K.; Shan, J.; Heinz, T. F., Control of Valley Polarization in Monolayer Mos₂ by Optical Helicity. *Nat. Nanotechnol.* **2012**, *7*, 494-498.
7. Zeng, H.; Dai, J.; Yao, W.; Xiao, D.; Cui, X., Valley Polarization in Mos₂ Monolayers by Optical Pumping. *Nat. Nanotechnol.* **2012**, *7*, 490-493.
8. Cao, T.; Wang, G.; Han, W.; Ye, H.; Zhu, C.; Shi, J.; Niu, Q.; Tan, P.; Wang, E.; Liu, B., *et al.*, Valley-Selective Circular Dichroism of Monolayer Molybdenum Disulphide. *Nat. Commun.* **2012**, *3*, 887.
9. Bertolazzi, S.; Brivio, J.; Kis, A., Stretching and Breaking of Ultrathin Mos₂. *ACS Nano* **2011**, *5*, 9703-9709.
10. Yin, Z.; Li, H.; Li, H.; Jiang, L.; Shi, Y.; Sun, Y.; Lu, G.; Zhang, Q.; Chen, X.; Zhang, H., Single-Layer Mos₂ Phototransistors. *ACS Nano* **2011**, *6*, 74-80.
11. Radisavljevic, B.; Whitwick, M. B.; Kis, A., Integrated Circuits and Logic Operations Based on Single-Layer Mos₂. *ACS Nano* **2011**, *5*, 9934-9938.
12. Kim, S.; Konar, A.; Hwang, W.-S.; Lee, J. H.; Lee, J.; Yang, J.; Jung, C.; Kim, H.; Yoo, J.-B.; Choi, J.-Y., *et al.*, High-Mobility and Low-Power Thin-Film Transistors Based on Multilayer Mos₂ Crystals. *Nat. Commun.* **2012**, *3*, 1011.
13. Wang, H.; Yu, L.; Lee, Y.-H.; Shi, Y.; Hsu, A.; Chin, M. L.; Li, L.-J.; Dubey, M.; Kong, J.; Palacios, T., Integrated Circuits Based on Bilayer Mos₂ Transistors. *Nano Lett.* **2012**, *12*, 4674-4680.
14. Li, H.; Yin, Z.; He, Q.; Li, H.; Huang, X.; Lu, G.; Fam, D. W. H.; Tok, A. I. Y.; Zhang, Q.; Zhang, H., Fabrication of Single- and Multilayer Mos₂ Film-Based Field-Effect Transistors for Sensing No at Room Temperature. *Small* **2012**, *8*, 63-67.
15. Pu, J.; Yomogida, Y.; Liu, K.-K.; Li, L.-J.; Iwasa, Y.; Takenobu, T., Highly Flexible Mos₂ Thin-Film Transistors with Ion Gel Dielectrics. *Nano Lett.* **2012**, *12*, 4013-4017.
16. He, Q.; Zeng, Z.; Yin, Z.; Li, H.; Wu, S.; Huang, X.; Zhang, H., Fabrication of Flexible Mos₂ Thin-Film Transistor Arrays for Practical Gas-Sensing Applications. *Small* **2012**, *8*, 2994-2999.
17. Lee, H. S.; Min, S.-W.; Chang, Y.-G.; Park, M. K.; Nam, T.; Kim, H.; Kim, J. H.; Ryu, S.; Im, S., Mos₂ Nanosheet Phototransistors with Thickness-Modulated Optical Energy Gap. *Nano Lett.* **2012**, *12*, 3695-3700.
18. Zhang, Y.; Ye, J.; Matsushashi, Y.; Iwasa, Y., Ambipolar Mos₂ Thin Flake Transistors. *Nano Lett.* **2012**, *12*, 1136-1140.
19. Novoselov, K. S.; Jiang, D.; Schedin, F.; Booth, T. J.; Khotkevich, V. V.; Morozov, S. V.; Geim, A. K., Two-Dimensional Atomic Crystals. *Proc. Nat. Acad. Sci. U.S.A.* **2005**, *102*, 10451-10453.

20. Goldberg, A. M.; Beal, A. R.; Lévy, F. A.; Davis, E. A., The Low-Energy Absorption Edge in 2h-Mos₂ and 2h-Mose₂. *Philos. Mag.* **1975**, *32*, 367-378.
21. Neville, R. A.; Evans, B. L., Band Edge Excitons in 2h-Mos-2. *Phys. Stat. Sol. B* **1976**, *73*, 597-606.
22. Wilson, J. A.; Yoffe, A. D., The Transition Metal Dichalcogenides: Discussion and Interpretation of the Observed Optical, Electrical and Structural Properties. *Adv. Phys.* **1969**, *18*, 193-335.
23. Braga, D.; Gutiérrez Lezama, I.; Berger, H.; Morpurgo, A. F., Quantitative Determination of the Band Gap of Ws₂ with Ambipolar Ionic Liquid-Gated Transistors. *Nano Lett.* **2012**, *12*, 5218-5223.
24. Fang, H.; Chuang, S.; Chang, T. C.; Takei, K.; Takahashi, T.; Javey, A., High-Performance Single Layered Wse₂ P-Fets with Chemically Doped Contacts. *Nano Lett.* **2012**, *12*, 3788-3792.
25. Kuc, A.; Zibouche, N.; Heine, T., Influence of Quantum Confinement on the Electronic Structure of the Transition Metal Sulfide Ts₂. *Phys. Rev. B* **2011**, *83*, 245213.
26. Yun, W. S.; Han, S. W.; Hong, S. C.; Kim, I. G.; Lee, J. D., Thickness and Strain Effects on Electronic Structures of Transition Metal Dichalcogenides: 2h-Mx₂ Semiconductors (M = Mo, W; X = S, Se, Te). *Phys. Rev. B* **2012**, *85*, 033305.
27. Jiang, H., Electronic Band Structures of Molybdenum and Tungsten Dichalcogenides by the Gw Approach. *J. Phys. Chem. C* **2012**, *116*, 7664-7671.
28. Zeng, H.; Liu, G.-B.; Dai, J.; Yan, Y.; Zhu, B.; He, R.; Xie, L.; Xu, S.; Chen, X.; Yao, W., *et al.*, Optical Signature of Symmetry Variations and Spin-Valley Coupling in Atomically Thin Tungsten Dichalcogenides. *arXiv:1208.5864* **2012**.
29. Gutierrez, H. R.; Perea-Lopez, N.; Elias, A. L.; Berkdemir, A.; Wang, B.; Lv, R.; Lopez-Urias, F.; Crespi, V. H.; Terrones, H.; Terrones, M., Extraordinary Room-Temperature Photoluminescence in Ws₂ Triangular Monolayers. *Nano Lett.* **2012**.
30. Li, H.; Lu, G.; Yin, Z.; He, Q.; Li, H.; Zhang, Q.; Zhang, H., Optical Identification of Single- and Few-Layer Mos₂ Sheets. *Small* **2012**, *8*, 682-686.
31. Zhao, W., Manuscript in Preparation.
32. Hecht, E., *Optics*. Addison-Wesley: Reading, MA, 1998.
33. Beal, A. R.; Knights, J. C.; Liang, W. Y., Transmission Spectra of Some Transition Metal Dichalcogenides. ii. Group VIA: Trigonal Prismatic Coordination. *J. Phys. C: Sol. Stat. Phys.* **1972**, *5*, 3540.
34. Bromley, R. A.; Murray, R. B.; Yoffe, A. D., The Band Structures of Some Transition Metal Dichalcogenides. iii. Group VIA: Trigonal Prism Materials. *J. Phys. C: Sol. Stat. Phys.* **1972**, *5*, 759.
35. Consadori, F.; Frindt, R. F., Crystal Size Effects on the Exciton Absorption Spectrum of Wse₂. *Phys. Rev. B* **1970**, *2*, 4893-4896.
36. Ramasubramaniam, A., Large Excitonic Effects in Monolayers of Molybdenum and Tungsten Dichalcogenides. *Phys. Rev. B* **2012**, *86*, 115409.
37. Mattheis, Lf, Band Structures of Transition-Metal-Dichalcogenide Layer Compounds. *Phys. Rev. B* **1973**, *8*, 3719-3740.
38. Yang, F.; Wilkinson, M.; Austin, E. J.; O'Donnell, K. P., Origin of the Stokes Shift: A Geometrical Model of Exciton Spectra in 2d Semiconductors. *Phys. Rev. Lett.* **1993**, *70*, 323-326.
39. Mak, K. F.; He, K.; Lee, C.; Lee, G. H.; Hone, J.; Heinz, T. F.; Shan, J., Observation of Tightly Bound Trions in Monolayer Mos₂. *arXiv:1210.8226*.
40. Voß, D.; Krüger, P.; Mazur, A.; Pollmann, J., Atomic and Electronic Structure of Wse₂ from Ab Initio Theory: Bulk Crystal and Thin Film Systems. *Phys. Rev. B* **1999**, *60*, 14311-14317.
41. Finteis, T.; Hengsberger, M.; Straub, T.; Fauth, K.; Claessen, R.; Auer, P.; Steiner, P.; Hüfner, S.; Blaha, P.; Vögt, M., *et al.*, Occupied and Unoccupied Electronic Band Structure of Wse₂. *Phys. Rev. B* **1997**, *55*, 10400-10411.
42. Traving, M.; Boehme, M.; Kipp, L.; Skibowski, M.; Starrost, F.; Krasovskii, E. E.; Perlov, A.; Schattke, W., Electronic Structure of Wse₂: A Combined Photoemission and Inverse Photoemission Study. *Phys. Rev. B* **1997**, *55*, 10392-10399.

43. Tongay, S.; Zhou, J.; Ataca, C.; Lo, K.; Matthews, T. S.; Li, J.; Grossman, J. C.; Wu, J., Thermally Driven Crossover from Indirect toward Direct Bandgap in 2d Semiconductors: MoSe_2 versus MoS_2 . *Nano Lett.* **2012**.
44. Wu, S.; Ross, J. S.; Aivazian, G.; Jones, A.; Fei, Z.; Liu, G.-B.; Zhu, W.; Xiao, D.; Yao, W.; Cobden, D., *et al.*, Electrical Tuning of Valley Magnetic Moment *via* Symmetry Control. *arXiv:1208.6069* **2012**.
45. Newaz, A. K. M.; Prasai, D.; Ziegler, J. I.; Caudel, D.; Robinson, S.; Jr, R. F. H.; Bolotin, K. I., Electrical Control of Optical Properties of Monolayer MoS_2 . *arXiv:1211.0341* **2012**.
46. Novoselov, K. S.; Neto, A. H. C., Two-Dimensional Crystals-Based Heterostructures: Materials with Tailored Properties. *Phys. Scr.* **2012**, *2012*, 014006.
47. Gao, G.; Gao, W.; Cannuccia, E.; Taha-Tijerina, J.; Balicas, L.; Mathkar, A.; Narayanan, T. N.; Liu, Z.; Gupta, B. K.; Peng, J., *et al.*, Artificially Stacked Atomic Layers: Toward New Van Der Waals Solids. *Nano Lett.* **2012**, *12*, 3518-3525.
48. Bernardi, M.; Palumbo, M.; Grossman, J. C., Semiconducting Monolayer Materials as a Tunable Platform for Excitonic Solar Cells. *ACS Nano* **2012**.
49. Wang, Q. H.; Kalantar-Zadeh, K.; Kis, A.; Coleman, J. N.; Strano, M. S., Electronics and Optoelectronics of Two-Dimensional Transition Metal Dichalcogenides. *Nat. Nanotechnol.* **2012**, *7*, 699-712.

Figures and Figure Captions

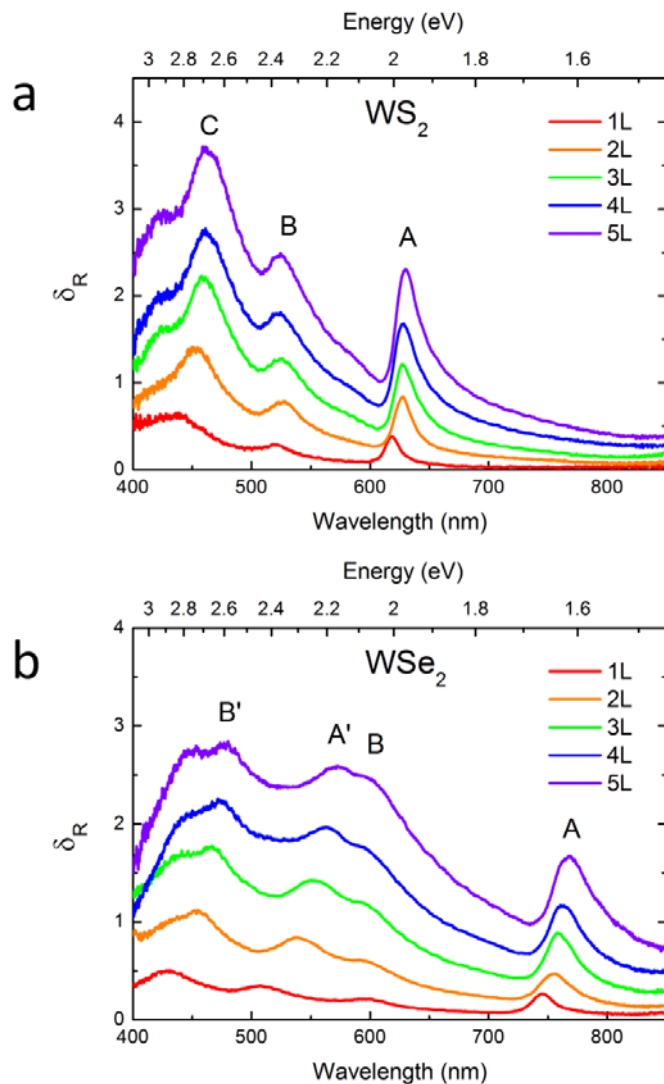


Figure 1 – Differential reflectance spectra of mechanically exfoliated (a) 2H- WS_2 and (b) 2H- WSe_2 flakes consisting of 1 to 5 layers. The peaks are labelled according to the convention proposed by Wilson and Yoffe²².

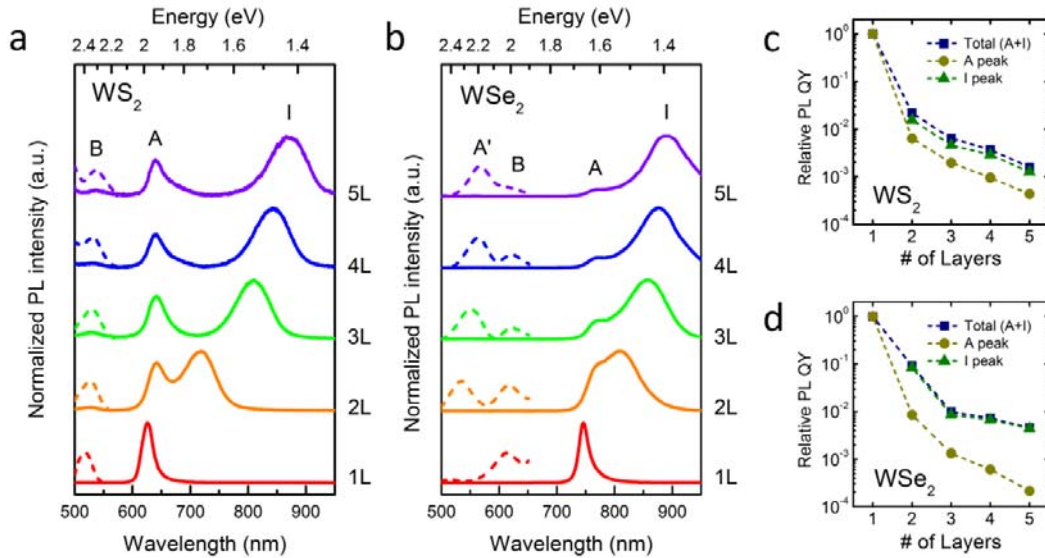


Figure 2 – Normalized photoluminescence spectra of mechanically exfoliated (a) 2H-WS₂ and (b) 2H-WSe₂ flakes consisting of 1 to 5 layers. Peak I is an indirect gap emission. Weak hot electron peaks A' and B are magnified as dashed lines for clarity. These hot electron peaks are typically 100 to 1000 times weaker than the band edge emission peaks. The total emission intensity becomes significantly weaker with increasing number of layers. Relative decay in the PL QY with the number of layers for (c) WS₂ and (d) WSe₂. The values are relative to the PL QY of a monolayer sample as discussed in the text. The plots are shown for A and I peaks and their sum (A+I).

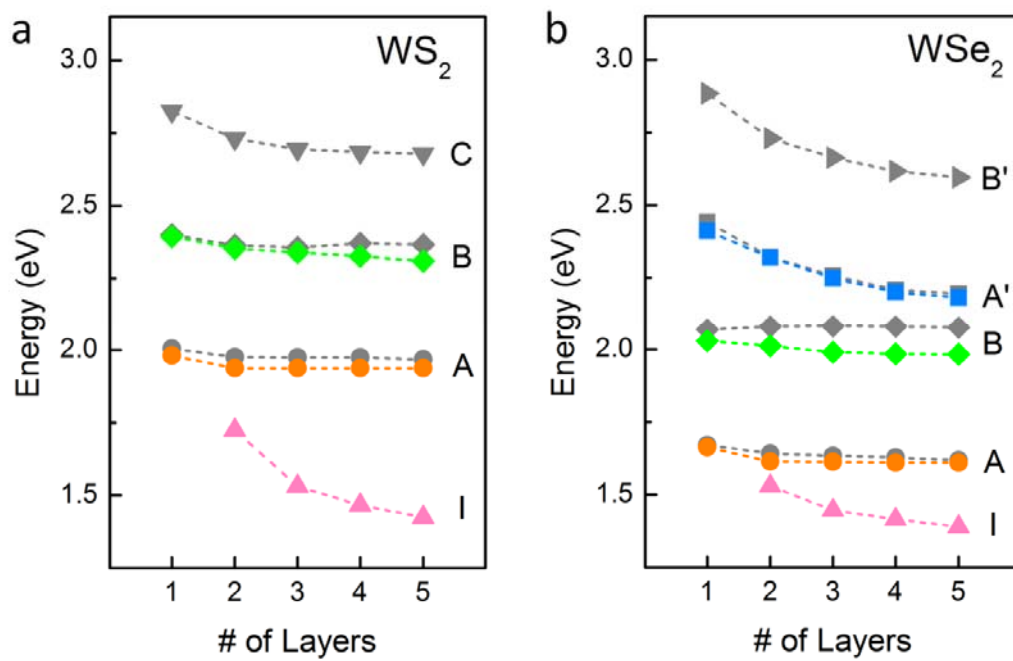


Figure 3 – Absorption (gray) and PL (color-coded) peak energies of (a) WS₂ and (b) WSe₂ flakes as a function of the number of layers. The letters I, A, B, A', B', and C refer to the peaks labeled in Figure 1 and 2.

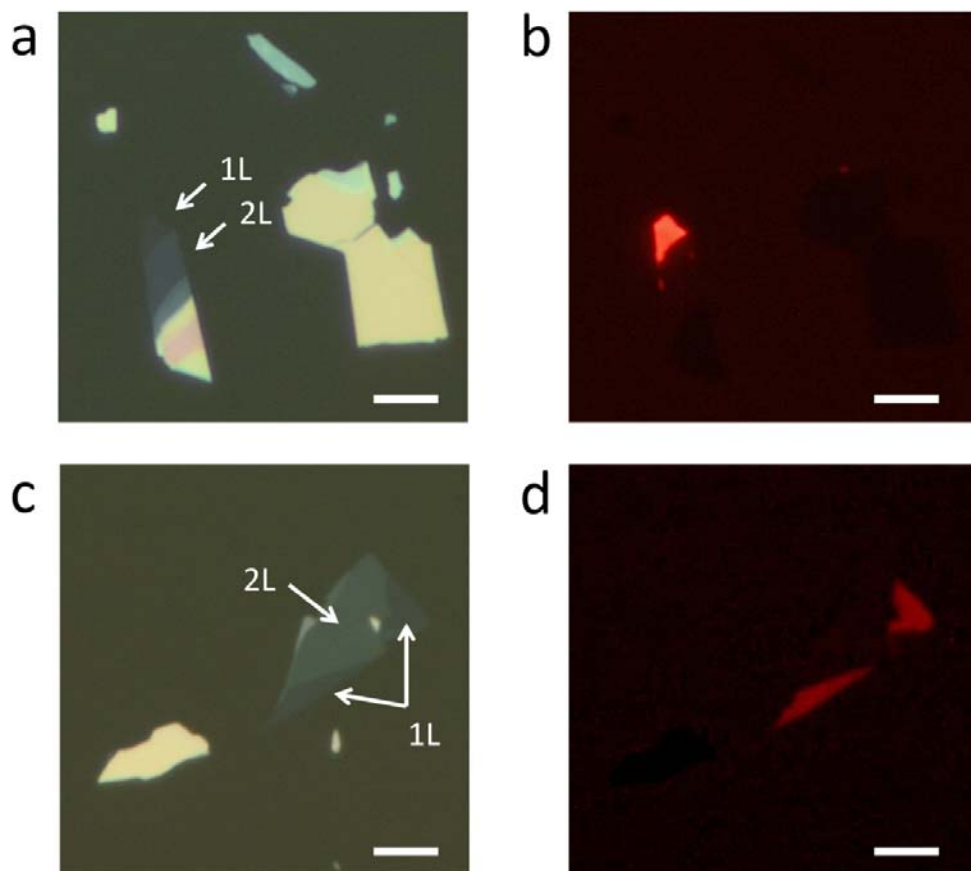


Figure 4 – Bright field optical images of mechanically exfoliated (a) WS₂ and (c) WSe₂ and their corresponding fluorescence images (b, d). The scale bar is 5 μm. The fluorescence images were obtained with excitation wavelength of 510-550 nm. Due to low efficiency of the CCD camera in the NIR range, fluorescence image contrast is artificially enhanced for WSe₂. The original image can be found in the Supporting Information.

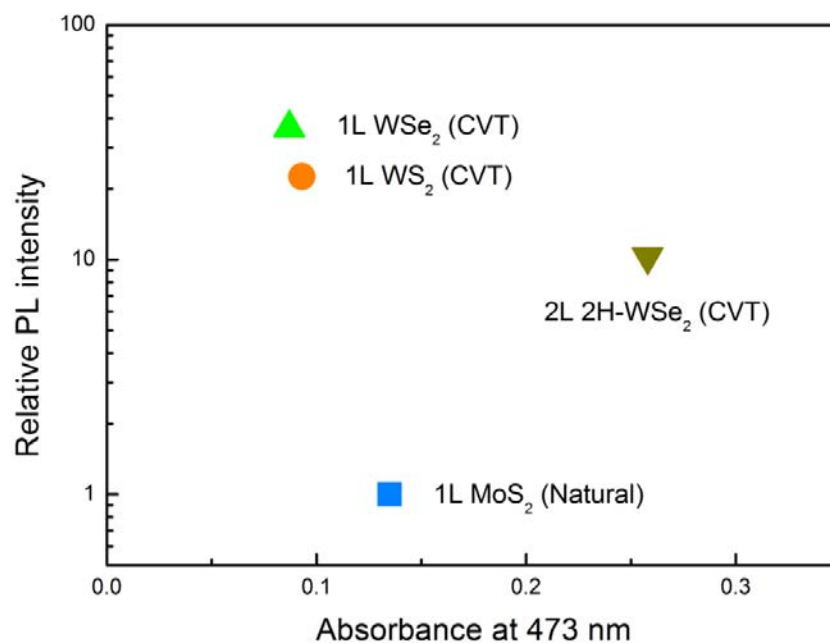


Figure 5 – Relative integrated PL intensity of WS₂ and WSe₂ monolayers and WSe₂ bilayer with respect to that of a MoS₂ monolayer plotted against absorbance at the excitation wavelength of 473 nm. The PL emission spectra were integrated over 520 to 950 nm. Absorbance is obtained from differential reflectance of samples on quartz based on Eqn 1. The absorbance of MoS₂ is obtained from Ref ⁵. Note that the comparison is made between exfoliated samples from synthetic (*i.e.* CVT-grown) WS₂/WSe₂ and natural MoS₂ (SPI supplies) crystals.

Supporting Information

Evolution of electronic structure in atomically thin sheets of WS_2 and WSe_2

Weijie Zhao^{a,c,#}, Zohreh Ghorannevis^{a,c,#}, Lei Qiang Chu^{a,c}, Minglin Toh^d, Christian Kloc^d, Ping Heng Tan^e, Goki Eda^{a,b,c,}*

^a Department of Physics, National University of Singapore, 2 Science Drive 3, Singapore 117542

^b Department of Chemistry, National University of Singapore, 3 Science Drive 3, Singapore 117543

^c Graphene Research Centre, National University of Singapore, 6 Science Drive 2, Singapore 117546

^d School of Materials Science and Engineering, Nanyang Technological University, N4.1 Nanyang Avenue, Singapore 639798

^e State Key Laboratory for Superlattices and Microstructures, Institute of Semiconductors, Chinese Academy of Sciences, Beijing, China, 100083

* E-mail: g.eda@nus.edu.sg

These authors contributed equally to this work.

1. AFM images

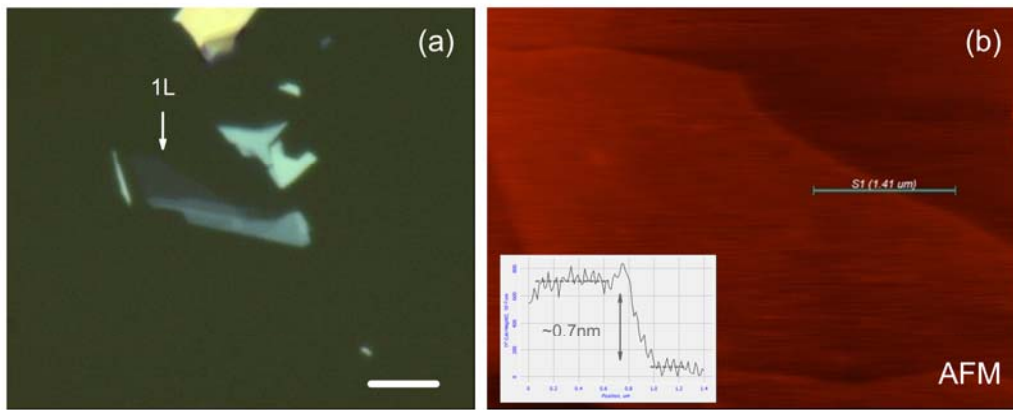


Figure S1 | Optical (a) and AFM (b) images of monolayer WS₂ on a quartz substrate. The scale bar in (a) is 5 μm.

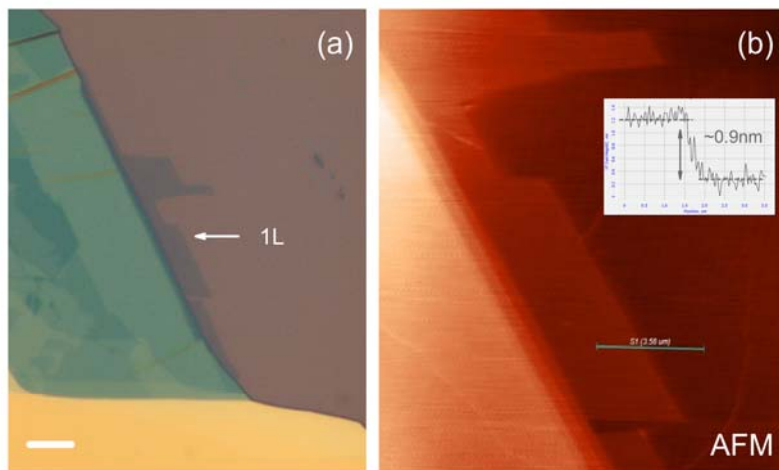


Figure S2 | Optical (a) and AFM (b) images of monolayer WSe₂ on a SiO₂/Si substrate. The scale bar in (a) is 5 μm.

2. Fluorescence images

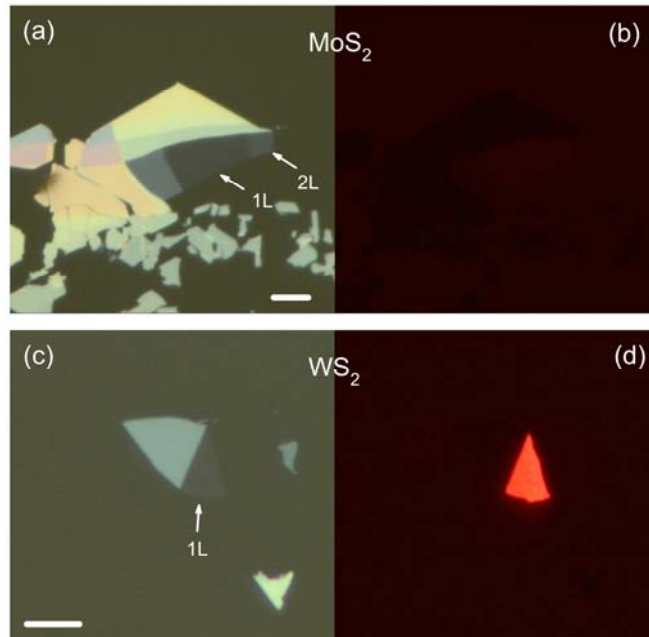


Figure S3 | Optical (a) and fluorescence (b) images of monolayer MoS₂. Optical (c) and fluorescence (d) images of monolayer WS₂. Both samples were deposited on a quartz substrate and the fluorescence images were taken under identical conditions. The scale bar in (a) and (c) is 5 μm .

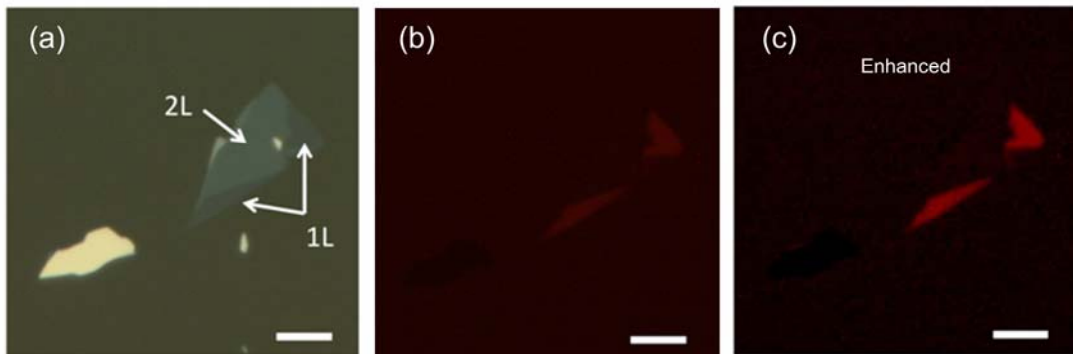


Figure S4 | Optical (a) and fluorescence (b) images of monolayer WSe₂ on quartz substrate. The fluorescence in (b) looks weak because of the low responsivity of the CCD of the fluorescence microscope in the near infrared range. Contrast

enhanced fluorescence image (c) is shown in Figure 4d of the main text. The scale bar is 5 μm .

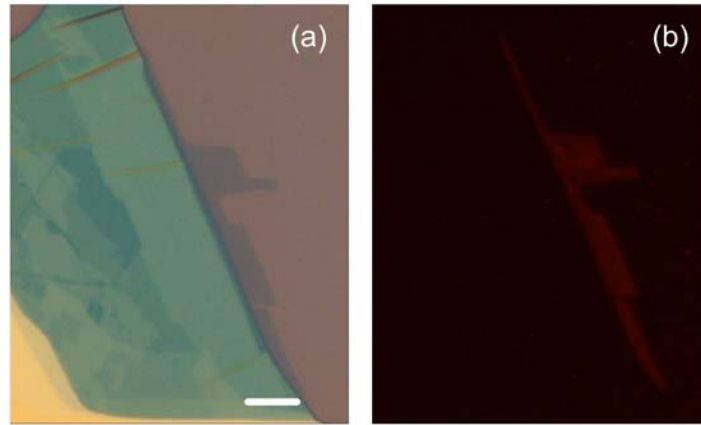


Figure S5 | Optical (a) and fluorescence (b) images of monolayer WSe_2 on a SiO_2/Si substrate. The scale bar in (a) is 5 μm .

3. Stokes shift

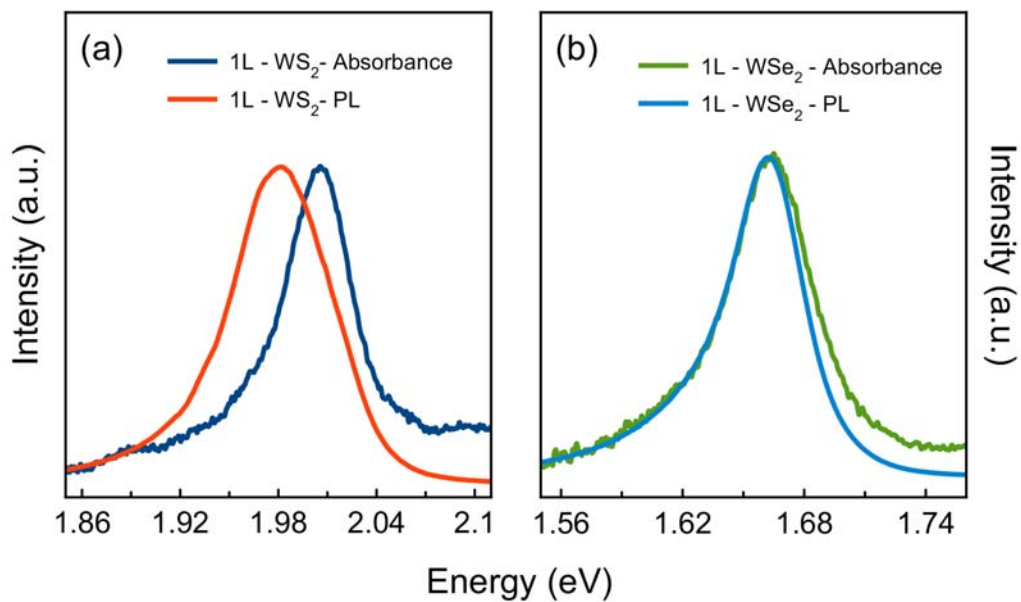


Figure S6 | Stokes shift of monolayer WS_2 (a) and WSe_2 (b). The absorbance spectra are equivalent to the differential reflectance spectra presented in the main text. The spectra are normalized and overlaid for clarity.